# Spatially restricted Hedgehog signaling regulates HGF-induced branching of the adult prostate

**Agnes Lim**[1,2,4,$], **Kunyoo Shin**[1,3,4,*,5,$], **Chen Zhao**[1,3,4], **Sally Kawano**[1,4], and **Philip A. Beachy**[1,2,3,4,*]

[1]Institute for Stem Cell Biology and Regenerative Medicine, Stanford University School of Medicine, Stanford, CA 94305

[2]Department of Developmental Biology, Stanford University School of Medicine, Stanford, CA 94305

[3]Department of Biochemistry, Stanford University School of Medicine, Stanford, CA 94305

[4]Howard Hughes Medical Institute, Stanford University School of Medicine, Stanford, CA 94305

## Abstract

Branching morphogenesis is thought to be governed by epithelial-stromal interactions, but the mechanisms underlying specification of branch location remain largely unknown. Prompted by the striking absence of Hedgehog (Hh) response at the sites of nascent buds in regenerating tubules of the adult prostate, we investigated the role of Hh signaling in adult prostate branching morphogenesis. We find that pathway activity is localized to stromal cells, and that its attenuation by genetic or pharmacologic manipulation leads to increased branching. Decreased pathway activity correlates with increased stromal production of Hepatocyte growth factor (Hgf), and we show that Hgf induces epithelial tubule branching. Regulation of Hgf expression by Hh signaling is indirect, mediated by Hh-induced expression of microRNAs miR-26a and miR-26b, which in turn down-regulate expression of Hgf. Prostate tubule branching thus may be initiated from regions of low Hh pathway activity, with implications for the prostatic hyperplasia commonly observed in late adulthood.

## Introduction

Epithelial-stromal interactions are crucial for normal pattern formation in embryonic organ development and for the homeostatic maintenance of organ integrity in adults. Following

[*]To whom correspondence may be addressed: Philip A. Beachy, pbeachy@stanford.edu, Tel: 650-723-4521, Fax: 650-725-7739. Lorry Lokey Stem Cell Institute. 265 Campus Drive. Stanford, CA, 94305; Kunyoo Shin, shink@ohsu.edu, Tel: 503-494-8958. Collaborative Life Sciences Builidng. 2730 SW Moddy Ave. Portland, OR, 97201.
[5]Current address: Department of Cell, Developmental, and Cancer Biology, Department of Urology, Oregon Health & Science University School of Medicine, Portland, OR 97239, USA
[$]These authors contributed equally to this work.

bacterial injury of the adult bladder, for example, Sonic hedgehog (Shh) produced in cells of the basal urothelium elicits production of secreted factors from stromal cells, which in turn stimulate proliferation and differentiation of urothelial cells. This epithelial/stromal signal feedback circuit underlies injury-induced regeneration of the urothelium and restoration of its normal function[1].

We focus here on growth and branching of the adult prostate. Our experimental system, the mouse prostate, comprises three paired lobes - the ventral, dorsolateral and anterior lobes - each consisting of a highly branched network of ductal tubules[2]. Castration results in loss of testosterone production and consequent involution of the prostate, largely through loss of distal branches. Testosterone replacement can then induce regeneration of new distal branches[3], thus providing a model for adult growth and branching morphogenesis.

Regenerative prostate growth in the adult differs significantly from embryonic and postnatal prostate development, as embryonic epithelium grows and invades an extensive expanse of mesenchyme that surrounds the epithelial ducts. In contrast, adult epithelial ducts are encircled by thin, dense, stromal sheaths which are in turn held together by looser interductal connective tissue[2]. The importance of understanding adult prostate regeneration is highlighted by the excessive branching and growth associated with benign prostatic hyperplasia, a condition affecting most men over 50 years of age[4].

Much previous study of the functional role of Hh signaling in prostate growth has focused on embryonic and early postnatal development[5–13] with contradictory reports of inhibitory effects of Hh signaling[9–11] or of decreased branching with Hh inhibition[12,13], and recent support for a changing role during development[8]. These studies have been based largely on *ex vivo* cultures of embryonic or early postnatal prostate from mice or rats treated with recombinant proteins or drugs. These *ex vivo* conditions do not fully recapitulate *in vivo* processes, especially responses that may be specifically restricted to epithelial or stromal cells, and the physiological significance of these studies thus requires *in vivo* validation. A common feature of all these studies is that Hh signal response normally occurs in stromal cells during embryonic[5,13] and early postnatal development[11], and in adulthood[14].

Although potential roles of Hh signaling during development have been suggested[5,6,8–13], detailed spatial information regarding Hh signal response in relation to branched outgrowth of adult prostate has not been presented. In addition, evidence from several studies suggests that there may be a shift in prevailing expression from *Sonic hedgehog* (*Shh*) in the embryo[11–13] to *Indian hedgehog* (*Ihh*) after birth[6]; production of Hh ligands from distinctly regulated genes thus may also contribute to distinct roles for Hh signaling in embryo and adult.

## Results

### Absence of stromal Hh response at the tips of nascent buds

Previous work showed that Hh pathway response, as determined by expression of the Hh pathway target gene *Gli1*, occurs only in a subset of stromal cells[14]. To visualize the three-dimensional organization of Hh response during prostate regeneration, *Gli1*^CreER/WT;

$R26^{\text{mTmG/WT}}$ mice were castrated to cause prostate regression followed two weeks later by insertion of a testosterone pellet to induce regeneration (Supplementary Fig. 1a). Tamoxifen (TM) was administered three days after testosterone replacement for a period of four days to activate CreER and thus induce excision of mT (membrane-targeted tdTomato), leading to permanent marking of *Gli1*-expressing cells and their progeny by expression of mG (membrane-targeted EGFP). Prostates were harvested three days later and treated with a clearing solution[15] to facilitate imaging of entire prostate ducts with two-photon microscopy, thus overcoming the limited imaging depth of confocal microscopy due to photo-bleaching and light scattering. Three-dimensional reconstruction of the two-photon images revealed that *Gli1*-positive, Hh-responsive cells are entirely stromal and are arranged in bands that enwrap the prostate tubules (Fig. 1a, Supplementary Fig. 1b and Supplementary Videos 1–4). Strikingly, Hh-response was conspicuously absent from stromal cells at the tips of nascent buds (best viewed in Supplementary Videos 1–4; see also Fig. 1a,b, and Supplementary Fig. 1b), but was present in stromal cells along the tubules, at branch points, or surrounding the ends of mature tubules that are not budding (Fig. 1c). These observations suggested that stromal regions lacking Hh pathway activity may promote formation of new prostate branches.

## Reduced Hh pathway activity increases tubulogenesis

To examine the role of Hh pathway activity in branch formation during prostate regeneration, *Gli1* mutant mice and wild type (WT) littermates were subjected to castration and androgen replacement (Fig. 2a), and three days later prostates were harvested. Each lobe was microdissected to display individual branches, which were counted and are presented as the % increase in branches relative to the number of tips that remain in involuted prostates. The % increase in branches upon regeneration more than doubled in $Gli1^{-/-}$ mutants relative to wild-type, with a 2.5-fold increase in the ventral prostate and a 2.9-fold increase in the dorsolateral prostate (Fig. 2b); attenuation of Hh pathway activity thus leads to increased prostate branching. Mice treated with the FDA-approved Smo antagonist, GDC-0449 (Vismodegib) beginning three days prior to androgen replacement and continuing throughout the duration of regeneration (Fig. 2c and Supplementary Fig. 1c) showed a 2.0-fold and 2.2-fold augmentation of the % increase in branches for the ventral and dorsolateral prostate, respectively, as compared to vehicle-treated mice (Fig. 2d).

Cell layer specificity of Hh action was examined by administering TM to mice expressing CreER under control of the *Gli1* promoter, which is active exclusively in stromal cells (see above); these mice also carried homozygous floxed alleles of the essential Hh pathway transductory component *Smoothened* (*Smo*) ($Gli1^{\text{CreER/WT}}$; $Smo^{\text{flox/flox}}$). With TM adminsitration prior to castration and testosterone replacement a similar 2.0-fold and 2.0-fold augmentation of the % increase in branching was observed in ventral and dorsolateral prostates respectively as compared to vehicle control mice (Fig. 2e,f and Supplementary Fig. 1d). Each of these three methods of Hh pathway attenuation consistently augments regenerative branching by at least 2-fold in an overall total of 60 samples and in a highly statistically significant manner. Attenuation of Hh pathway activity thus promotes branching, and the critical site of this effect is in the stromal cells that enwrap the growing tubules.

## Hh pathway activity in stromal cells reduces Hgf levels

As branching morphogenesis necessarily involves the epithelium, we hypothesized that the effect of stromal Hh pathway response on prostate branching is mediated by a secreted factor. We performed a microarray analysis of RNA extracted from wild type or *Gli1* mutant prostates after castration and 3 days of androgen replacement and found that 85 genes were up-regulated by at least 1.4-fold (p<0.01) in regenerating *Gli1* mutant prostates as compared to WT. We selected genes annotated with the SP_PIR_Keyword "signal" and "secreted" to identify genes encoding secreted proteins involved in cell signaling (Supplementary Table 1) and found *Hepatocyte growth factor (Hgf)* as an attractive candidate for a prostate branching factor because it modulates branching of mammary gland[16,17], lung[18] and kidney[19]. We confirmed the microarray data by RT-PCR (Fig. 3a), and found that Hgf protein levels were also significantly higher in *Gli1* mutant prostates as compared to WT (Fig. 3b).

To investigate the cell layer specificity of gene expression we used an established FACS protocol to isolate epithelial basal and luminal cells as well as stromal cells from WT prostates (Fig. 3c)[20] and immediately subjected them to RT-PCR analysis (Fig. 3d); stromal cell identity was confirmed by culture and staining with antibodies against vimentin and smooth muscle actin (SMA) (Fig. 3e). As expected, *Gli1* is expressed primarily in stromal cells, which is also the predominant site of *Hgf* expression (Fig. 3d). Expression of the Hgf receptor c-Met in contrast was highest in epithelial cells, predominantly the basal fraction (Fig. 3d).

To directly determine if Hh pathway activity in stromal cells modulates *Hgf* levels, cultured stromal cells were treated with the Smoothened agonist, purmorphamine, or DMSO as a control (Fig. 3f). Following 24 hours of purmorphamine treatment we noted an increase in *Gli1* transcripts; we also noted a corresponding decrease in levels of *Hgf* mRNA and in levels of HGF protein secreted into the medium (Fig. 3f). In addition, treatment with purmorphamine of NIH 3T3 cells, a mouse embryo fibroblast line known both to produce Hgf[21] and to respond to Hh signaling[22], led to decreased activity of conditioned medium in an MDCK cell tubulogenesis assay[23,24] (Supplementary Fig. 2), consistent with a negative regulatory effect of Hh signaling on *Hgf* expression. Taken together, these data indicate an inhibitory relationship between Hh pathway activity and stromal levels of Hgf.

This relationship, in combination with two-photon images of regenerating prostates (Fig. 1a and Supplementary Fig. 1b), raise the interesting possibility that regions where stromal cells lack Hh response may correspond to regions with high levels of Hgf at the locations of new branches. To test this hypothesis, *Gli1*[CreER/WT]; *R26*[EYFP/WT] mice were castrated, testosterone pellets implanted, and three days later TM was administered on four consecutive days to label *Gli1*-expressing cells during regeneration. Following an additional three days for completion of TM-induced recombination, prostates were harvested and EYFP-positive and -negative stromal cells isolated by FACS (Fig. 3g). RT-PCR analyses of RNA extracted from these cells showed an increase in *Gli1* and *Ptch1* mRNA levels in the EYFP-positive cells (Fig. 3g), indicating that the population is enriched for cells that are responding to the Hh ligand. These EYFP-positive cells expressed lower levels of *Hgf* than EYFP-negative cells (Fig. 3g), suggesting that regions of low Hh response are regions of

higher *Hgf* expression. The level of expression of the stromal marker *Vimentin* was unchanged between the two populations.

The difference in *Gli1* mRNA between EYFP-positive and -negative stromal cells in this experiment, although clear and statistically significant, is not as great as in isolated stromal cells stimulated *in vitro*, possibly resulting from the 3–6 days between TM administration and prostate harvest. During this elapsed time Hh response patterns may change as branching and maturation of the regenerating prostate tubules proceeds, leading to an underestimate of the difference in pathway activity and in *Hgf* expression in isolated cells as compared to the actual difference *in vivo* at the time of recombination and marking.

### Hgf induces prostate branching

To determine whether Hgf induces prostate branching, dissociated prostate cells were cultured *in vitro* in three-dimensional cultures for 5 days until they formed spheres (Fig. 4a), after which recombinant Hgf protein was added to the media. Four days later we observed the formation of complex branched structures in Hgf-treated wells, but not in control conditions (Fig. 4b,c and Supplementary Video 5), demonstrating that Hgf acts on the prostate epithelium to induce branching morphogenesis. To investigate the possibility that Hgf induces prostate branching by stimulating cell proliferation, basal prostate epithelial cells were isolated and cultured *in vitro* until they formed small colonies, at which time recombinant Hgf protein was added. Two days later we found 1.9-fold more Hgf-treated cells, as compared to the control (Supplementary Fig. 3a), suggesting that Hgf indeed stimulates cell proliferation.

To further test if stromal *Hgf* expression induces branching, we utilized a subrenal prostate regeneration assay, which involves engraftment of adult prostate epithelium and embryonic urogenital sinus mesenchyme (UGSM) under the kidney capsule of immunocompromised mice[20,25–27]. UGSM cells were transduced with a bicistronic lentiviral construct for expression of Hgf, and GFP from an internal ribosome entry site. GFP-positive UGSM cells were isolated by FACS, and combined in equal proportion with adult epithelial cells expressing membrane-tagged tdTomato (Fig. 4d). Examination of tissue sections through these subrenal prostate grafts 8 weeks after implantation revealed a 1.9-fold greater number of tubules in grafts formed from UGSM infected with lentivirus expressing *Hgf* as compared to the control grafts (Fig. 4e,f,g), indicative of increased branching stimulated by increased *Hgf* levels.

To directly examine the role of Hgf signaling response in prostate branching, we utilized mice expressing CreER under control of the ubiquitously expressed *Actin* promoter to drive deletion of a conditional c-Met allele[28] (*ActinCreER; c-Met*flox/flox); deletion of c-Met following TM administration was verified by genotyping DNA from prostate lobes (Supplementary Fig. 3b). *ActinCreER; c-Met*flox/flox or *c-Met*flox/flox mice were castrated, then treated with TM after prostate regression. Testosterone pellets were implanted three days later to allow completion of TM-induced recombination, and prostates were dissected five days after that (Fig. 5a). As compared to control *c-Met*flox/flox mice, *ActinCreER; c-Met*flox/flox mice showed a 3.7-fold and a 3.3-fold attenuation in % increase in branches of ventral and dorsolateral prostate, respectively (Fig. 5b). These results demonstrate that

reduction of Hgf response *in vivo* leads to dramatically decreased branching morphogenesis during regeneration.

To confirm this pharmacologically, WT mice were castrated, and then treated with a c-Met inhibitor, AMG 458, prior to androgen replacement (Fig. 5c). AMG 458 is an orally bioavailable drug that is highly specific for c-Met, showing selectivity for inhibition of c-Met over a panel of tyrosine and serine/threonine kinases[29]; we indeed noted a reduction of phosphorylated c-Met protein in drug-treated mice as compared to controls (Supplementary Fig. 3c). Five days after androgen replacement, animals treated with AMG 458 showed ventral and dorsolateral prostates with 1.8-fold and 1.4-fold attenuation respectively in % increase in branches as compared to vehicle-treated animals (Fig. 5d). These *in vitro* and *in vivo* genetic and pharmacologic data together show that Hgf signaling plays a crucial role in promoting adult prostate branching.

## Hh pathway down-regulates *Hgf* via miR-26a/b

Hh and Hgf pathway activities have opposite effects on prostate branching, and Hh pathway activity is associated with decreased *Hgf* expression, suggesting a negative regulatory relationship between Hh activity and expression of *Hgf*. The Hh pathway mediator Gli1, however, functions exclusively as a transcriptional activator[30], suggesting an indirect relationship between Gli1 and *Hgf* expression. To investigate whether this could occur via Hh-pathway activation of microRNA transcription, potential microRNAs that could target *Hgf* were identified using the TargetScanMouse 6.2[31] and DIANA-microT 3.0[32,33] algorithms. Both prediction algorithms had as their top-ranked hits the paralogs miR-26a and miR-26b, which have identical seed sequences (6–8 nucleotides at the 5′ end of the mature miRNA) and may target the same regions on the 3′ UTR of *Hgf* mRNA. In addition to complementarity of the seed sequence to the *Hgf* 3′ UTR, both miRNAs also have a supplementary site at the 3′ end of the miRNA, which is complementary to the *Hgf* UTR and is thought to augment seed pairing[34]. Both miRNAs are predicted to target two sites on the 3′ UTR of *Hgf*, with identical seed sequences and slightly different supplementary sequences, and both sites are highly conserved in vertebrate *Hgf* 3′ UTRs (Fig. 6a and Supplementary Fig. 4).

To determine if miR-26a and miR-26b are able to regulate the 3′ UTR of *Hgf*, luciferase reporter assays were used (Fig. 6b). The 3′ UTR of *Hgf* was cloned into the pMir-Report vector, downstream of the luciferase gene. HEK293S cells were co-transfected with Renilla luciferase vector and the pMir-Report luciferase vector with or without the *Hgf* 3′ UTR, and with mature miR-26a or miR-26b mimics, which are chemically modified double-stranded RNAs that mimic endogenous mature miRNAs. Co-transfection of miR-26a or miR-26b mimics suppressed the luciferase activity of the vector with the *Hgf* 3′UTR by 45% and 30% respectively compared to a negative control scrambled mimic, but did not change the luciferase levels of the control vector (Fig. 6c). Mutation of the seed region in both sites of the *Hgf* 3′ UTR abrogated the repressive effect of the miRNA mimics, demonstrating the specificity of the miRNA mimics for *Hgf* (Fig. 6c).

In addition to the *Hgf* 3′ UTR, the ability of miR-26a and miR-26b to regulate endogenous *Hgf* mRNA and protein levels in prostate stromal cells was examined. Stromal cells were

isolated from WT mouse prostates by FACS and cultured *in vitro*, transfected with miRNA mimics, and *Hgf* mRNA and protein levels determined (Fig. 6d). Transfection of either miR-26a or miR-26b led to a decrease in both *Hgf* mRNA and protein levels as compared to transfection with a scrambled miRNA mimic, demonstrating that both miRNAs are able to regulate endogenous *Hgf* levels in prostate cells (Fig. 6e,f).

To test the possibility that Hh pathway activity reduces *Hgf* levels by increasing miR-26a and miR-26b expression, we treated WT prostate stromal cells with purmorphamine and found that levels of both miR-26a and miR-26b increased upon purmorphamine treatment (Fig. 6g,h). We also isolated stromal cells from regenerating prostates based on their status of Hh pathway response, by isolating EYFP-positive and EYFP-negative cells from regenerating *Gli1*$^{CreER/WT}$; *R26*$^{EYFP/WT}$ prostates (Fig. 3g). EYFP expression indicates response to Hh ligand (Fig. 3g), and we find that these cells also express increased levels of miR-26a and miR-26b (Fig. 6i) and decreased levels of *Hgf* (Fig. 3g), providing further evidence that Hh pathway activity down-regulates *Hgf* levels via miR-26a and miR-26b.

### Ihh expression patterns stromal Hh response

To determine whether expression of *Gli1* in a restricted subset of stromal cells results from differential response to the Hh ligand within stromal cells or, alternatively, from restricted Hh ligand expression in epithelial cells, we isolated *Gli1*-positive and -negative cells from *Gli1*$^{CreER/WT}$; *R26*$^{EYFP/WT}$ mice that were given TM. EYFP-positive and -negative prostate stromal cells were isolated by FACS, cultured separately *in vitro*, stimulated with purmorphamine, and levels of *Gli1* transcript were measured by RT-PCR (Supplementary Fig. 5a). We found that both EYFP-positive and -negative cells responded to purmorphamine by upregulating *Gli1* expression to similar extents (Supplementary Fig. 5b), indicating that all stromal cells retain an equivalent capacity to respond to Hh pathway stimulation, and suggesting possible differences in Hh ligand expression.

Although Peng et al. showed that basal cells at the proximal end of the prostate dorsal lobe express *Shh*[14], others have shown that *Shh* expression in the prostate is greatly down-regulated after birth[11,13], whereas *Ihh* expression persists[6]. Our own RT-PCR analyses of *Shh* and *Ihh* mRNA levels in RNA extracted from embryonic (E15.5), early post-natal (P2) and adult ventral and dorsolateral prostate lobes showed that, during development, *Shh* mRNA levels progressively declined ~10-fold relative to internal controls whereas *Ihh* mRNA levels progressively increased by ~12-fold. The ~120-fold change in the relative abundance of *Ihh* mRNA as compared to *Shh* mRNA from embryo to adult suggests that their relative importance as ligands may shift during development (Fig. 7a and Supplementary Fig. 5c). Indeed, we examined prostates of TM-treated *Shh*$^{CreER/WT}$; *R26*$^{mTmG/WT35}$ mouse adults and did not detect expression of Shh in the distal regions (Supplementary Fig. 5e). Primary adult prostate stromal cells in culture respond to recombinant Ihh protein by up-regulating expression of *Gli1*, miR-26a and mir-26b, and down-regulating *Hgf* expression (Supplementary Fig. 5d), and the increased levels of adult *Ihh* expression and the prominence of distal prostate in adult regenerative branching morphogenesis together suggest that *Ihh* may play an important role in patterning Hh

pathway response in the stroma, thereby controlling the local levels of stromal *Hgf* expression.

To determine whether the pattern of *Ihh* expression in the prostate is similar to the pattern of *Gli1* expression, we generated an *Ihh*^CreER^ mouse with *CreER* knocked into the endogenous *Ihh* locus (Supplementary Fig. 6). TM was administered to *Ihh*^CreER/WT^; *R26*^mTmG/WT^ and *Gli1*^CreER/WT^; *R26*^mTmG/WT^ mice, and prostates were harvested after five days. Examination of tissue sections from *Gli1*^CreER/WT^; *R26*^mTmG/WT^ prostates showed ductal regions wholly or partially surrounded by stromal cells that are *Gli1*-positive and thus are responding to Hh ligand, but also ductal regions surrounded by *Gli1*-negative stromal cells (Fig. 7b). Tissue sections from *Ihh*^CreER/WT^; *R26*^mTmG/WT^ prostates revealed similar patterns of *Ihh* expression in the epithelium, with some regions entirely or partially *Ihh*-positive, as well as other regions entirely devoid of *Ihh* expression. These similarities suggest that the pattern of *Gli1* expression in prostate stroma could be accounted for by the pattern of *Ihh* expression (Fig. 7b). The regional differences in *Ihh*^CreER^-driven marking are not likely due to incomplete Cre recombination as the dose and duration of TM treatment, when administered to *ActinCreER; R26*^mTmG/WT^ mice, induced almost 100% recombination in epithelial cells (Fig. 7b).

## Discussion

In this study we find that Hh response in regenerating prostate is present in the stromal cells that enwrap prostate tubules, but is conspicuously absent from stromal cells at the sites of nascent tubule buds. These stromal cells lacking Hh response express higher levels of *Hgf* than Hh-responsive stromal cells, an effect likely mediated by Hh induction of miR26a and miR26b. We find that Hgf stimulates prostate branching, thus providing a link between reduced Hh response in specific regions of the stroma and the sites of epithelial branching. Finally, we find that the spatial pattern of Hh signal response in stromal cells is strikingly similar to the pattern of *Indian hedgehog* (*Ihh*) expression in the epithelium, suggesting that the location of nascent buds during adult prostate branching morphogenesis is specified by spatially restricted Hh signaling from epithelium to stroma.

Our data suggest a model (Fig. 8a) in which regional differences in Hh ligand secretion and pathway response determine the location of a nascent bud during adult branching morphogenesis. Thus, in epithelial regions of high *Ihh* expression, Hh response in adjacent stromal cells down-regulates stromal expression of *Hgf* by inducing expression of miR-26a and miR-26b (Fig. 8b), leading to low concentrations of Hgf ligand and a consequent lack of branching. Regions of low epithelial Ihh ligand expression in contrast would be associated with low Hh response in adjacent stromal cells, permitting high levels of Hgf secretion that could stimulate formation of nascent buds.

Although a branched structure is essential for normal prostate function, the occurrence of excessive branching in adulthood is associated with benign prostatic hyperplasia (BPH), a disease that affects 50% of men in their 50s and increases progressively to 90% of men in their 80s[4]. BPH is characterized by an increase in nodules in the transition zone of the human prostate due to excessive ductal budding and branching[36–39]. Currently, there are two

generally accepted permissive factors for the pathogenesis of BPH, the presence of circulating androgens and increasing age[40], but the underlying molecular mechanisms remain poorly understood. The epithelial/stromal interaction described here appears likely to operate in human prostate, as *Shh* ligand expression in the normal human prostate is localized to the epithelium, whereas pathway response, as determined by *Gli1* expression is localized to the stroma[41]. *c-Met* expression is localized to the basal cells in both normal human transition zone and in BPH samples[42], and cultured prostate stromal cells *in vitro* secrete *Hgf*[43]. The Hh/Hgf circuit we describe thus might be involved in driving the abnormal prostate growth observed in BPH; alternatively, this circuit may simply operate to pattern the branching in the context of growth that is driven by other factors. In either case, manipulation of this epithelial/stromal feedback circuit could prove therapeutically useful.

## Methods

### Mice

Male mice between 8 and 10 weeks of age were used for all experiments. $Gli1^{LacZ/WT}$ heterozygotes[44] from our colony were back-crossed for 10 generations to the FVB strain, then interbred to generate $Gli1^{LacZ/LacZ}$ homozygotes. Wild-type littermates were used as controls. $Gli1^{CreER/WT}$ mice[45] were crossed with $R26^{EYFP/EYFP}$ mice[46] or $R26^{mTmG/mTmG}$ mice[47] or $Smo^{flox/flox}$ mice[48] to obtain $Gli1^{CreER/WT}$; $R26^{EYFP/WT}$ or $Gli1^{CreER/WT}$; $R26^{mTmG/WT}$ or $Gli1^{CreER/WT}$; $Smo^{flox/WT}$ mice. Resulting mice were crossed with $Smo^{flox/flox}$ mice to obtain $Gli1^{CreER/WT}$; $Smo^{flox/flox}$ mice. All mouse strains except as otherwise indicated were obtained from Jackson Laboratories. All castration and testosterone implantation procedures were performed under isoflurane anaesthesia, which was administered in a fume hood with a standard vaporizer (J. B. Baulch and Associates). To induce CreER-mediated recombination in mice harboring the CreER allele, tamoxifen (Sigma, 12 mg per 30 g body weight) was administered by oral gavage. For each experiment, no statistical method was used to predetermine sample size, and mice in each cage were randomly selected for drug/TM or control treatments. The investigators were blinded to allocation during experiments and outcome assessment. Counting of prostate tubules was blinded to ensure that the investigator who assessed the tissues did not know which treatment group each sample belonged to. All procedures were performed under a protocol approved by the Administrative Panel on Laboratory Animal Care at Stanford University. In all experiments, only the ventral and dorsolateral lobes of the prostate were analyzed.

### Castration and testosterone replacement

Castration was performed by ligation of the spermatic cord and complete removal of the testes and epididymides through a scrotal approach. 14 days after castration, a pellet of testosterone (Innovative Research of America, SA-151, 10 mg) was implanted subcutaneously in the back of the mouse.

### Two-photon imaging

$Gli1^{CreER/WT}$; $R26^{mTmG/WT}$ mice were castrated and testosterone replaced after 2 weeks. 3 days after testosterone replacement, tamoxifen (Sigma, 12 mg per 30 g body weight) was

administered by oral gavage daily for 4 consecutive days. 3 days after the last dose, individual prostate lobes were dissected, fixed in 4% paraformaldehyde for 24 h, washed twice in PBS and incubated in ScaleA2 solution containing 4M urea, 10% (wt/vol) glycerol and 0.1% (wt/vol) Triton X-100[15] for 2 weeks at 4°C. Images were captured using the Prairie Ultima IV upright two-photon microscope. Three-dimensional reconstructions of two-photon images were generated using Imaris software (Bitplane Scientific Software).

### Branching analysis

Individual prostate lobes were dissected in PBS and incubated in 1% collagenase (Sigma C6885) for 15 minutes at room temperature with gentle agitation. After rinsing in PBS, individual branches of each lobe were separated using fine forceps, and images captured using a Leica M205 FA Stereomicroscope. The number of branch tips in each lobe was counted manually. The difference between the number of branches in a regenerating prostate lobe and the average number of branches in a pool of regressed prostate lobe from equivalent mice (giving the number of new branches) was divided by the number of branches in the regressed lobe and expressed as a percentage increase in the number of new branches. All prostate regeneration experiments involving branching analyses were performed on pairs of mice (control and treatment/mutant) with the same protocol on the same day to reduce variability. Pairs of mice were castrated on the same day, in the same manner, and the prostates allowed to regress. After 2 weeks, testosterone pellets were implanted subcutaneously on the same day for each pair of mice, and the prostates harvested and analyzed together on the same day.

### Microarray analysis

$Gli1$[LacZ/LacZ]and WT littermates were castrated and testosterone replaced after 2 weeks. 3 days after testosterone replacement, the mice were sacrificed, prostate lobes harvested, and total RNA was prepared using the RNeasy Plus Mini Kit (Qiagen). RNA quality was evaluated using the Agilent 2100 Bioanalyzer system. Samples were hybridized to the Affymetrix GeneChip Mouse Exon 1.0 ST microarray chips. Three mice of each genotype were analyzed. After hybridization, expression values were normalized using the RMA function in the Partek Genomics Suite software. Differentially expressed genes were identified using ANOVA, genes showing a fold change greater or equal to 1.4 with P-value < 0.01 were shortlisted for functional annotation analyses. Examination of Swiss-Prot (SP) and Protein Information Resource (PIR) Keywords (SP_PIR_KEYWORDS) was performed using DAVID[49] (http://david.abcc.ncifcrf.gov/). Expression changes detected by microarray analysis were validated using quantitative RT-PCR.

### Database accession number

The microarray data set is available in the GEO database (GEO accession: GSE59849).

### AMG 458 treatment

FVB mice were castrated. After 13 days, a 30mg/kg of body weight dose of AMG 458 in HPMCT (2% hydroxypropylmethylcellulose, 1% Tween-80 in water, adjusted to pH 2.2 with HCl) or vehicle alone was administered by oral gavage [29]. A dose of AMG 458 or

vehicle was administered 12 h and 24 h later. 6 h after the third dose, a testosterone pellet was implanted subcutaneously and fourth dose was administered 6 h later. AMG 458 or vehicle alone was administered twice daily for 5 d after testosterone implantation. Prostates were harvested 3 h after the last dose, and processed for branching analyses. For protein extraction, a portion of the left lobe of the liver was removed, homogenized in RIPA buffer (50 mM Tris-HCl pH8, 150 mM NaCl, 1% Triton-X 100, 0.5% Sodium deoxycholate, 0.1% SDS, 1 mM EGTA) with Halt Protease and Phosphatase Inhibitor Cocktail (Pierce 78440), incubated at 4°C for 30 min, centrifuged at 10,000g for 30 min and the supernatant removed. 15 μg of total protein was loaded into each lane for SDS/PAGE and Western blotting with a rabbit anti-phospho-c-Met antibody (Invitrogen 44888G, 1:1000) or mouse anti-β-tubulin (Sigma T8660, 1:1000) antibody. Densitometric analysis of Western blot bands was performed using Image J software (NIH).

### GDC-0449 treatment

FVB mice were castrated. After 11 days, a 100 mg/kg of body weight dose of GDC-0449 in MCT (0.5% methylcellulose, 0.2% Tween-80)[50] or vehicle only control was administered by oral gavage twice a day for 3 d. 6 h after the last dose, testosterone was implanted subcutaneously, and GDC-0449 or vehicle was administered 6 h later, then twice daily for 3 d after testosterone implantation. Prostates were harvested 3 h after the last dose. For each paired lobe of the prostate, one lobe was processed for branching analyses and the other was homogenized for RNA extraction.

### Immunofluorescence analysis of tissue sections

Individual prostate lobes were dissected in PBS, fixed in 4% paraformaldehyde for 6 hours, washed 3 times in PBS, incubated in 30% sucrose overnight, then embedded and snap-frozen in OCT compound (Tissue-tek). 12 μm sections were obtained using a Leica cryostat. For immunostaining, tissue sections were rinsed in PBS twice, then blocked in 10% goat serum in PBS containing 2% BSA and 0.25% Triton X-100 for 1 h, and incubated with the following primary antibodies diluted in blocking solution overnight at 4°C in a humidified chamber: rabbit anti-GFP (Invitrogen A11122, 1:500), chicken anti-vimentin (Millipore, 1:600). Sections were washed three times with PBS containing 0.25% Triton X-100, incubated with DAPI and appropriate Alexa fluor -conjugated secondary antibodies diluted 1:1,000 in blocking solution for 1h at 22°C, washed again three times, and mounted on slides with Prolong Gold mounting reagent (Invitrogen). Immunofluorescence images presented are images from one representative experiment of three.

### Immunofluorescence analysis of cultured cells

Stromal cells were isolated by FACS and plated onto 18-mm diameter circular coverslips in 12-well plates, and fixed 4% paraformaldehyde for 20 min. Cells were permeabilized with PBS/0.5% Triton X-100 for 3 min and nonspecific binding sites were blocked with 2% BSA in PBST (PBS with 0.5% Tween- 20) for 1 h. Cells were stained with primary antibodies: chicken anti-vimentin (Millipore AB5733, 1:600) and mouse anti-smooth muscle actin (Sigma 1A4, 1:1000) diluted in 2% BSA/PBST for 1 h at room temperature. After washing four times in PBST, cells were incubated for 1 h with appropriate Alexa fluor 488 or 594-conjugated secondary antibodies (Invitrogen, 1:1000) together with 1 g/mL of 4,6-

diamidino-2-phenylindole (DAPI) for nuclear staining in 2% BSA/PBST. Cells were washed four times in PBST, then mounted on slides with Prolong Gold mounting reagent (Invitrogen). Immunofluorescence images presented are images from one representative experiment of three.

### Fluorescence-activated cell sorting (FACS)

Prostate lobes were dissociated and stained for FACS based on published methods[20]. Briefly, prostate lobes were dissected, minced, and incubated at 37°C in 10%FBS/DMEM containing 1 mg/ml collagenase (Gibco, cat. no. 17018–029). Further dissociation to a single cell suspension was achieved by incubation in Trypsin/0.05% EDTA (Invitrogen cat. no. 25300) for 5 minutes at 37°C, followed by serially passing through 18-G and 20-G needles and filtering through a nylon mesh filter with a 40 μm pore size. Cells were stained for 20 minutes at 4°C. Antibodies used are: Sca-1-APC (clone D7; eBioscience, cat. no. 17–5981–82), 1:500; Ter119-FITC (clone TER-119; eBioscience, cat. no. 11–5921–85), 1:250; CD31-FITC (clone 390; eBioscience, cat. no. 11–0311–85), 1:250; CD45-FITC (clone 30-F11; eBioscience, cat. no. 11–0451–85), 1:250; CD49f-PE (clone eBioGoH3; eBioscience, cat. no. 12–0495–83) 1:333. Cells were sorted using a FACS AriaII cytometer (BD Biosciences), and analysis of flow cytometry data was performed using FlowJo Software (Treestar). Following FACS, isolated cells were centrifuged at 500g for 5 minutes. The pellet washed in PBS, homogenized in lysis buffer from the RNAqueous-Micro RNA Isolation Kit (Ambion AM1931), the mirVana miRNA Isolation Kit (Ambion AM1560) and RNA extracted following kit instructions.

### Stromal cell culture and Hgf ELISA

FACS-isolated stromal cells were cultured in 10% FBS/DMEM in a 48-well tissue culture plate. When the cells were 80% confluent, old media was removed and cells were incubated in 150 μl 10% FBS/DMEM containing 10 μM purmorphamine (Calbiochem 540220) or DMSO control. In separate experiments, cultured stromal cells were treated with 10% FBS/DMEM containing 5 μg/ml recombinant Ihh protein (R&D 1705-HH-025) in 0.1% BSA or a BSA only control. In separate experiments, cells were transfected with miRNA mimics for miR-26a (Ambion, Assay MC10249) or miR-26b (Ambion, Assay MC12899) or a negative control (Ambion 4464076). After 22 h, media was removed and centrifuged at 10,000g for 5 min. To measure the concentration of Hgf in the media, 10 μl of the supernatant was used in each well of the Mouse/Rat HGF Quantikine ELISA Kit (R&D Systems, MHG00) and the plate processed according to manufacturer's instructions. Each sample was analyzed in duplicate.

### Protein extraction from prostate lobes

Individual prostate lobes were dissected in PBS, washed, and homogenized in PBS using a pestle. An equal volume of Lysis Buffer 2 (R&D 895347) was added and the homogenate incubated at room temperature for 30 min with agitation. The lysate was centrifuged at 10,000g for 30 min at 4°C, and the supernatant removed. Protein levels in each extract was determined using the Quick Start Bradford 1x Dye Reagent (Bio-Rad 500–0205), equal amounts of total protein were loaded into each well of the Mouse/Rat HGF Quantikine ELISA Kit (R&D Systems, MHG00) and the plate processed according to manufacturer's

instructions. Each sample was analyzed in duplicate, and Hgf levels for each sample was normalized to total protein in each well.

## Quantitative RT-PCR

Prostate lobes were dissected in RNase-free PBS, and placed immediately in lysis buffer from the mirVana miRNA Isolation Kit (Ambion AM1560) or RNeasy Plus Mini Kit (Qiagen 74134). Cells were homogenized in lysis buffer using a pestle, and RNA extracted following respective kit instructions. Colon and bladder samples were snap-frozen in liquid nitrogen, homogenized using a mortar and pestle, and RNA extracted using the RNeasy Plus Mini Kit (Qiagen). For quantitative RT-PCR of mRNA transcripts, first-strand cDNA was made using SuperScript III First-Strand Synthesis SuperMix (Invitrogen 18080–400). Quantitative RT-PCR was performed using iQ SYBR Green Supermix (Bio-Rad 170–8880) and the Bio-Rad iCycler. All assay values were normalized to the *HPRT1* internal control.

For quantitative RT-PCR of mature miRNA, cDNA was made using the TaqMan MicroRNA Reverse Transcription Kit (Applied Biosystems) and primers from respective TaqMan MicroRNA Assays according to manufacturer's instructions. Quantitative RT-PCR was performed using the TaqMan Universal PCR Master Mix (Applied Biosystems 4324018), TaqMan MicroRNA Assays for miR-26a (Applied Biosystems, Assay 000405) or miR-26b (Applied Biosystems, Assay 000407) or Sno202 (Applied Biosystems, Assay 001232) and the Applied Biosystems 7300 Real-Time PCR System. All assay values were normalized to the Sno202 internal control.

## Conditioned medium from NIH 3T3 fibroblasts

Conditioned media was prepared by incubating 100% confluent NIH 3T3 fibroblasts (ATCC) with 5% BCS containing 10 μM purmorphamine (Calbiochem 540220) or DMSO control. After 72 h, media was collected and passed through a 0.22 μm filter to remove cell debris. 3T3 cells were washed in PBS and RNA was extracted using the RNeasy Plus Mini Kit (Qiagen).

## MDCK tubulogenesis

Madin-Darby canine kidney (MDCKII) cells (ATCC) were mixed with 170 μl ice cold Geltrex Matrix (Gibco A1413201), layered onto 12-mm Transwell clear filters and allowed to solidify at 37°C. Pre-warmed DMEM containing 10% FBS was added above and below the wells. Media was changed every 3 d. When cysts were formed (7 d after plating), tubulogenesis was induced using a 1:1 mix of 5% FBS and conditioned media from NIH 3T3 cells treated with DMSO or purmorphamine. Media was changed daily, and cysts were analyzed after 6 d. The percentage of cysts that formed extensions in 10 fields of view per well was determined, and 4 wells were analyzed for each type of conditioned medium. For staining of the cysts, cysts were recovered from the Geltrex Matrix by incubating in Cell Recovery Solution (BD Biosciences 354253) on ice for 1 h. After centrifugation at 300g for 5 min, the pellet containing the cysts was washed with PBS and fixed with 4% paraformaldehyde for 20 min at 22°C. After washing in PBS, cysts were stained with Alexa Fluor 594 phalloidin (Invitrogen A12381, 1:25) and DAPI in 10% goat serum in PBS containing 2% BSA and 0.25% Triton X-100 at 4°C overnight. Cysts were washed in PBS

containing 0.25% Triton X-100 thrice and mounted on slides in Cytoseal mounting reagent (Thermo Scientific 23–244257). Immunofluorescence images presented are images from one representative experiment of three.

### Confocal microscopy

Immunofluorescence images were obtained using a Zeiss LSM 510 inverted confocal microscope and prepared for publication with Zeiss LSM 5 Image Browser software and Adobe Photoshop CS4.

### Generation of miRNA target reporter constructs

The full length 3′ UTR of Hgf (corresponding to position 2310–2755 of the RefSeq sequence NM_010427) and both fragments of 3′UTR each containing a putative miR-26a/b target sequence (corresponding to positions 2363–2428 and 2508–2588 of the RefSeq sequence NM_010427) were amplified by PCR using cDNA from adult murine prostate cells as a template and primers that introduced a SpeI and HindIII cut site at the 5′ and 3′ end of the PCR product respectively. Each PCR product was inserted downstream of the luciferase gene in the pMir-Report vector using the SpeI and HindIII cut sites. All products were sequenced. Mutation of the putative miR-26a/b target sequence within the 3′UTR of Hgf was generated using the QuikChange Site-Directed Mutagenesis kit (Stratagene).

### Luciferase reporter assays

HEK293S cells were seeded at $1 \times 10^5$ cells per well in 24-well plates the day prior to transfection. All transfections were carried out with Lipofectamine 2000 (Invitrogen), according to the manufacturer's instructions. Cells were transfected with 80 ng of pMir-Report luciferase expression construct containing the 3′UTR of murine Hgf, 20 ng pRL-SV40 Renilla luciferase vector (Promega E2231) and 100 nM miR-26a mirVana miRNA mimic (Ambion, Assay MC10249) or miR-26b mimic (Ambion, Assay MC12899) or negative control miRNA mimic (Ambion 4464076). 24 h after transfection, luciferase activities were measured using the Dual-Luciferase Reporter Assay System (Promega) and normalized to Renilla luciferase activity. All experiments were performed in triplicate.

### *In vitro* tubulogenesis assay

Adult prostates from WT or $R26^{mTmG}$ mice were harvested, dissociated, mixed with neutralized collagen (BD Biosciences), plated out in 48 well plates ($5 \times 10^4$ cells per well), and 500 μl of PrEGM (Lonza) was added. Media was changed after 3 days. 5 days from the start of culture, PrEGM was replaced with PrEBM (Lonza) containing hydrocortisone (5 μg/ml) and insulin/transferrin/selenium (Gibco) with or without Hgf (50 ng/ml). Media was changed after 3 days and cells were imaged the following day. One representative experiment of three is presented.

### *In vitro* cell proliferation assay

Adult prostates from WT were harvested, dissociated and plated out in 96 well plates ($10^4$ cells per well), and 500ul of PrEGM (Lonza) was added. After 3 days, PrEGM was replaced with PrEBM (Lonza) containing hydrocortisone (5 μg/ml) and insulin/transferrin/selenium

(Gibco) with or without Hgf (50 ng/ml). Cells were imaged after 3 days. To quantify the number of cells in each well, cells were trypsinized and counted using a haemocytometer.

### Subrenal capsule prostate grafts

Subrenal capsule graft experiments were performed as previously described[20]. Briefly, adult prostates from $R26^{mTmG}$ mice were harvested, dissociated and basal and luminal cells isolated by FACS. Urogenital sinus mesenchyme (UGSM) was harvested from E16.5 embryos, passaged twice *in vitro*, then infected with lentivirus expressing Hgf-IRES-GFP. 24 hours after infection, UGSM were washed, trypsinized and GFP-positive and GFP-negative cells were isolated by FACS. For the control grafts, $2\times10^5$ GFP-negative cells were combined with a total of $2\times10^5$ basal and luminal cells in equal proportion in neutralized collagen. For experimental grafts, $10^5$ GFP-negative and $10^5$ GFP-positive UGSM were combined with total of $2\times10^5$ basal and luminal cells in equal proportion. Grafts were implanted into the renal capsule of anesthetized SCID/SCID mice and a testosterone pellet (Innovative Research of America, 12.5 mg) was inserted subcutaneously. Grafts were harvested 8 weeks later for analysis. One representative experiment of two is presented.

### Generation of the *Ihh*^CreER mouse strain

A bacterial artificial chromosome (BAC) clone containing the *Ihh* gene locus was obtained, and genetic modifications of the clone were performed using the Gene Bridges Quick and Easy BAC Modification kit (Cat #K001) according to the manufacturer's protocol. A CreER-FRT-Neo-FRT cassette was inserted into the locus, replacing the ATG start codon of Ihh with the ATG codon of CreER. Mutation-free, successfully modified BAC clones were subcloned into a minimal vector, linearized by digestion with ScaI, then electroporated into R1 mouse embryonic stem cells (ESCs) Correctly targeted clones were identified by Southern blotting, karyotyped, and microinjected into 2–8 cell stage embryos. Heterozygous progeny from germ-line transmitting chimeric mice were mated with R26-FlpO mice in order to excise the FRT-flanked Neo cassette in the targeted *Ihh* allele to generate the final *Ihh*^CreER strain.

### Statistical analysis

Statistical analysis was performed using GraphPad Prism software v.5. All data are presented as mean ± s.e.m., and two group comparisons were done with a two-tailed Student's t-test. A value of $P < 0.05$ was taken as statistically significant. Paired t-tests were used to compare regenerating prostates because pairs of age-matched and weight-matched test and control animals were analyzed on the same day, and only one pair of animals was analyzed per day. All other t-tests were unpaired.

## Supplementary Material

Refer to Web version on PubMed Central for supplementary material.

## Acknowledgments

## References

1. Shin K, et al. Hedgehog/Wnt feedback supports regenerative proliferation of epithelial stem cells in bladder. Nature. 2011; 472:110–114. [PubMed: 21389986]

2. Sugimura Y, Cunha GR, Donjacour AA. Morphogenesis of ductal networks in the mouse prostate. Biol Reprod. 1986; 34:961–971. [PubMed: 3730488]

3. Sugimura Y, Cunha G, Donjacour A. Morphological and histological study of castration-induced degeneration and androgen-induced regeneration in the mouse prostate. Biol Reprod. 1986; 34:973. [PubMed: 3730489]

4. Paolone DR. Benign prostatic hyperplasia. Clinics in geriatric medicine. 2010; 26:223–239. [PubMed: 20497842]

5. Berman DM, et al. Roles for Hedgehog signaling in androgen production and prostate ductal morphogenesis. Dev Biol. 2004; 267:387–398. [PubMed: 15013801]

6. Doles J, et al. Functional compensation in Hedgehog signaling during mouse prostate development. Dev Biol. 2006; 295:13–25. [PubMed: 16707121]

7. Karhadkar SS, et al. Hedgehog signalling in prostate regeneration, neoplasia and metastasis. Nature. 2004; 431:707–712. [PubMed: 15361885]

8. Yu M, Bushman W. Differential stage-dependent regulation of prostatic epithelial morphogenesis by Hedgehog signaling. Dev Biol. 2013; 380:87–98. [PubMed: 23660337]

9. Freestone S, et al. Sonic hedgehog regulates prostatic growth and epithelial differentiation. Dev Biol. 2003; 264:352–362. [PubMed: 14651923]

10. Wang BE, et al. Inhibition of epithelial ductal branching in the prostate by sonic hedgehog is indirectly mediated by stromal cells. J Biol Chem. 2003; 278:18506–18513. [PubMed: 12626524]

11. Pu Y, Huang L, Prins G. Sonic hedgehog-patched Gli signaling in the developing rat prostate gland: lobe-specific suppression by neonatal estrogens reduces ductal growth and branching. Dev Biol. 2004; 273:257–275. [PubMed: 15328011]

12. Podlasek C, Barnett D, Clemens J, Bak P, Bushman W. Prostate development requires Sonic hedgehog expressed by the urogenital sinus epithelium. Dev Biol. 1999; 209:28–39. [PubMed: 10208740]

13. Lamm M, et al. Sonic hedgehog activates mesenchymal Gli1 expression during prostate ductal bud formation. Dev Biol. 2002; 249:349–366. [PubMed: 12221011]

14. Peng YC, Levine CM, Zahid S, Wilson EL, Joyner AL. Sonic hedgehog signals to multiple prostate stromal stem cells that replenish distinct stromal subtypes during regeneration. Proceedings of the National Academy of Sciences. 2013; 110:20611–20616.

15. Hama H, et al. Scale: a chemical approach for fluorescence imaging and reconstruction of transparent mouse brain. Nat Neurosci. 2011; 14:1481–1488. [PubMed: 21878933]

16. Niranjan B, et al. HGF/SF: a potent cytokine for mammary growth, morphogenesis and development. Development. 1995; 121:2897–2908. [PubMed: 7555716]

17. Soriano JV, Pepper MS, Nakamura T, Orci L, Montesano R. Hepatocyte growth factor stimulates extensive development of branching duct-like structures by cloned mammary gland epithelial cells. Journal of Cell Science. 1995; 108(Pt 2):413–430. [PubMed: 7768990]

18. Ohmichi H, Koshimizu U, Matsumoto K, Nakamura T. Hepatocyte growth factor (HGF) acts as a mesenchyme-derived morphogenic factor during fetal lung development. Development. 1998; 125:1315–1324. [PubMed: 9477330]

19. Santos OFP, et al. Involvement of Hepatocyte Growth Factor in Kidney Development. Dev Biol. 1994; 163:525–529. [PubMed: 8200486]

20. Lukacs RU, Goldstein AS, Lawson DA, Cheng D, Witte ON. Isolation, cultivation and characterization of adult murine prostate stem cells. Nature Protocols. 2010; 5:702–713. [PubMed: 20360765]

21. Stoker M, Gherardi E, Perryman M, Gray J. Scatter factor is a fibroblast-derived modulator of epithelial cell mobility. Nature. 1987; 327:239–242. [PubMed: 2952888]

22. Taipale J, et al. Effects of oncogenic mutations in Smoothened and Patched can be reversed by cyclopamine. Nature. 2000; 406:1005–1009. [PubMed: 10984056]

23. Montesano R, Matsumoto K, Nakamura T, Orci L. Identification of a fibroblast-derived epithelial morphogen as hepatocyte growth factor. Cell. 1991; 67:901–908. [PubMed: 1835669]

24. Montesano R, Schaller G, Orci L. Induction of epithelial tubular morphogenesis in vitro by fibroblast-derived soluble factors. Cell. 1991; 66:697–711. [PubMed: 1878968]

25. Lawson D, Xin L, Lukacs R, Cheng D, Witte O. Isolation and functional characterization of murine prostate stem cells. Proceedings of the National Academy of Sciences. 2007; 104:181.

26. Goldstein AS, et al. Trop2 identifies a subpopulation of murine and human prostate basal cells with stem cell characteristics. Proceedings of the National Academy of Sciences. 2008; 105:20882–20887.

27. Wang X, et al. A luminal epithelial stem cell that is a cell of origin for prostate cancer. Nature. 2009; 461:495–500. [PubMed: 19741607]

28. Huh CG. Hepatocyte growth factor/c-met signaling pathway is required for efficient liver regeneration and repair. Proc Natl Acad Sci USA. 2004; 101:4477–4482. [PubMed: 15070743]

29. Liu L, et al. Discovery of a Potent, Selective, and Orally Bioavailable c-Met Inhibitor: 1-(2-Hydroxy-2-methylpropyl)- N-(5-(7-methoxyquinolin-4-yloxy)pyridin-2-yl)-5-methyl-3-oxo-2-phenyl-2,3-dihydro-1 H-pyrazole-4-carboxamide (AMG 458). J Med Chem. 2008; 51:3688–3691. [PubMed: 18553959]

30. Dai P, et al. Sonic Hedgehog-induced Activation of the Gli1Promoter Is Mediated by GLI3. J Biol Chem. 1999; 274:8143–8152. [PubMed: 10075717]

31. Lewis BP, Burge CB, Bartel DP. Conserved Seed Pairing, Often Flanked by Adenosines, Indicates that Thousands of Human Genes are MicroRNA Targets. Cell. 2005; 120:15–20. [PubMed: 15652477]

32. Maragkakis M, et al. Accurate microRNA target prediction correlates with protein repression levels. BMC Bioinformatics. 2009; 10:295. [PubMed: 19765283]

33. Maragkakis M, et al. DIANA-microT web server: elucidating microRNA functions through target prediction. Nucleic Acids Research. 2009; 37:W273–W276. [PubMed: 19406924]

34. Bartel DP. MicroRNAs: target recognition and regulatory functions. Cell. 2009; 136:215–233. [PubMed: 19167326]

35. Harfe B, et al. Evidence for an expansion-based temporal Shh gradient in specifying vertebrate digit identities. Cell. 2004; 118:517–528. [PubMed: 15315763]

36. Mcneal JE. Pathology of benign prostatic hyperplasia. Insight into etiology. Urol Clin North Am. 1990; 17:477–486. [PubMed: 1695776]

37. McNeal JE. Origin and evolution of benign prostatic enlargement. Invest Urol. 1978; 15:340–345. [PubMed: 75197]

38. Price H, Mcneal JE, Stamey TA. Evolving patterns of tissue composition in benign prostatic hyperplasia as a function of specimen size. Human Pathology. 1990; 21:578–585. [PubMed: 2351388]

39. Lee KL, Peehl DM. Molecular and cellular pathogenesis of benign prostatic hyperplasia. J Urol. 2004; 172:1784–1791. [PubMed: 15540721]

40. Untergasser G, Madersbacher S, Berger P. Benign prostatic hyperplasia: age-related tissue-remodeling. Exp Gerontol. 2005; 40:121–128. [PubMed: 15763388]

41. Fan L, et al. Hedgehog signaling promotes prostate xenograft tumor growth. Endocrinology. 2004; 145:3961. [PubMed: 15132968]

42. Pisters LL, et al. c-met proto-oncogene expression in benign and malignant human prostate tissues. J Urol. 1995; 154:293–298. [PubMed: 7539865]

43. Nakashiro K, Okamoto M, Hayashi Y, Oyasu R. Hepatocyte growth factor secreted by prostate-derived stromal cells stimulates growth of androgen-independent human prostatic carcinoma cells. American Journal of Pathology. 2000; 157:795. [PubMed: 10980119]

44. Bai C, Auerbach W, Lee J, Stephen D, Joyner A. Gli2, but not Gli1, is required for initial Shh signaling and ectopic activation of the Shh pathway. Development. 2002; 129:4753. [PubMed: 12361967]

45. Ahn S, Joyner A. Dynamic changes in the response of cells to positive hedgehog signaling during mouse limb patterning. Cell. 2004; 118:505–516. [PubMed: 15315762]

46. Srinivas S, et al. Cre reporter strains produced by targeted insertion of EYFP and ECFP into the ROSA26 locus. BMC Developmental Biology. 2001; 1:4. [PubMed: 11299042]

47. Muzumdar MD, Tasic B, Miyamichi K, Li L, Luo L. A global double-fluorescent Cre reporter mouse. Genesis. 2007; 45:593–605. [PubMed: 17868096]

48. Long F, Zhang XM, Karp S, Yang Y, Mcmahon AP. Genetic manipulation of hedgehog signaling in the endochondral skeleton reveals a direct role in the regulation of chondrocyte proliferation. Development. 2001; 128:5099–5108. [PubMed: 11748145]

49. Huang DW, et al. DAVID Bioinformatics Resources: expanded annotation database and novel algorithms to better extract biology from large gene lists. Nucleic Acids Research. 2007; 35:W169–W175. [PubMed: 17576678]

50. Robarge K, et al. GDC-0449--A potent inhibitor of the hedgehog pathway. Bioorganic & medicinal chemistry letters. 2009; 19:5576–5581. [PubMed: 19716296]
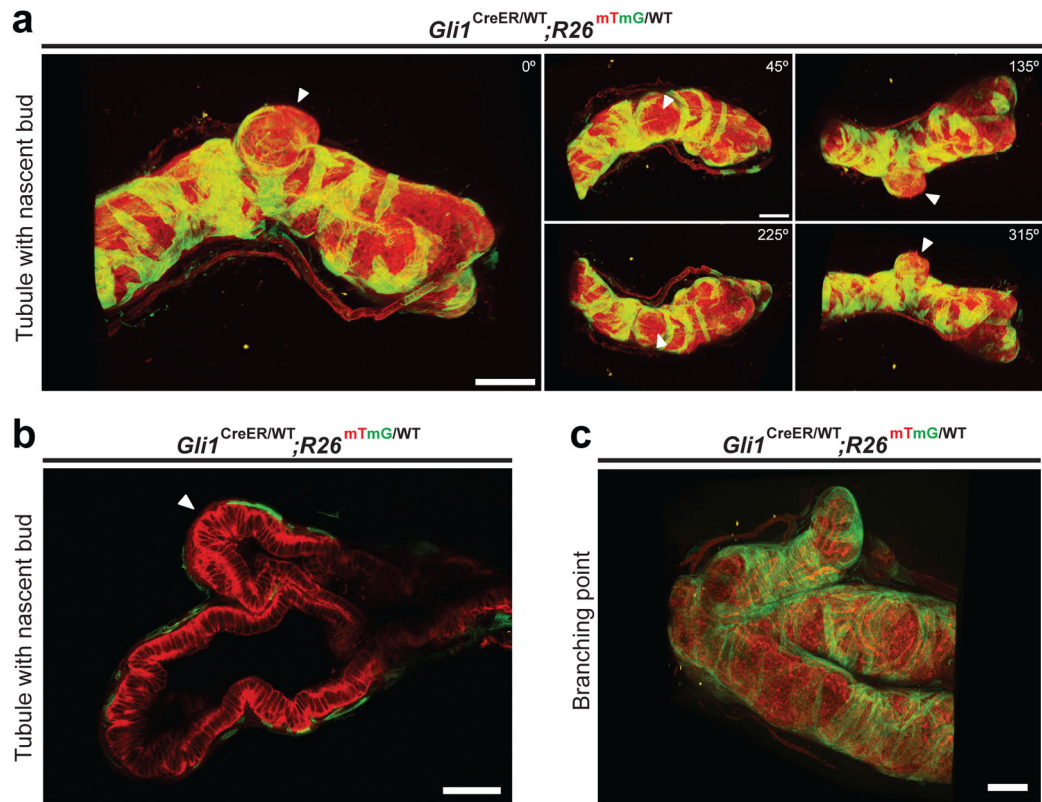
**Figure 1. Absence of stromal Hh response at the tips of nascent buds**
(a,c) Three-dimensional reconstruction of two-photon images of a regenerating prostate tubule from a *Gli1*$^{CreER/WT}$; *R26*$^{mTmG}$ prostate. (a) Arrowheads indicate the location of a nascent bud, which lacks *Gli1*-positive cells. Numbers indicate the degree of rotation of the tubule relative to the starting position. (c) A branch point with three mature tubules. *Gli1*-positive cells are located at the branch points and along tubules. (b) Optical section through a nascent bud, showing the absence of *Gli1*-positive stromal cells at the bud tip (arrowhead). Scale bars represent 100 μm.
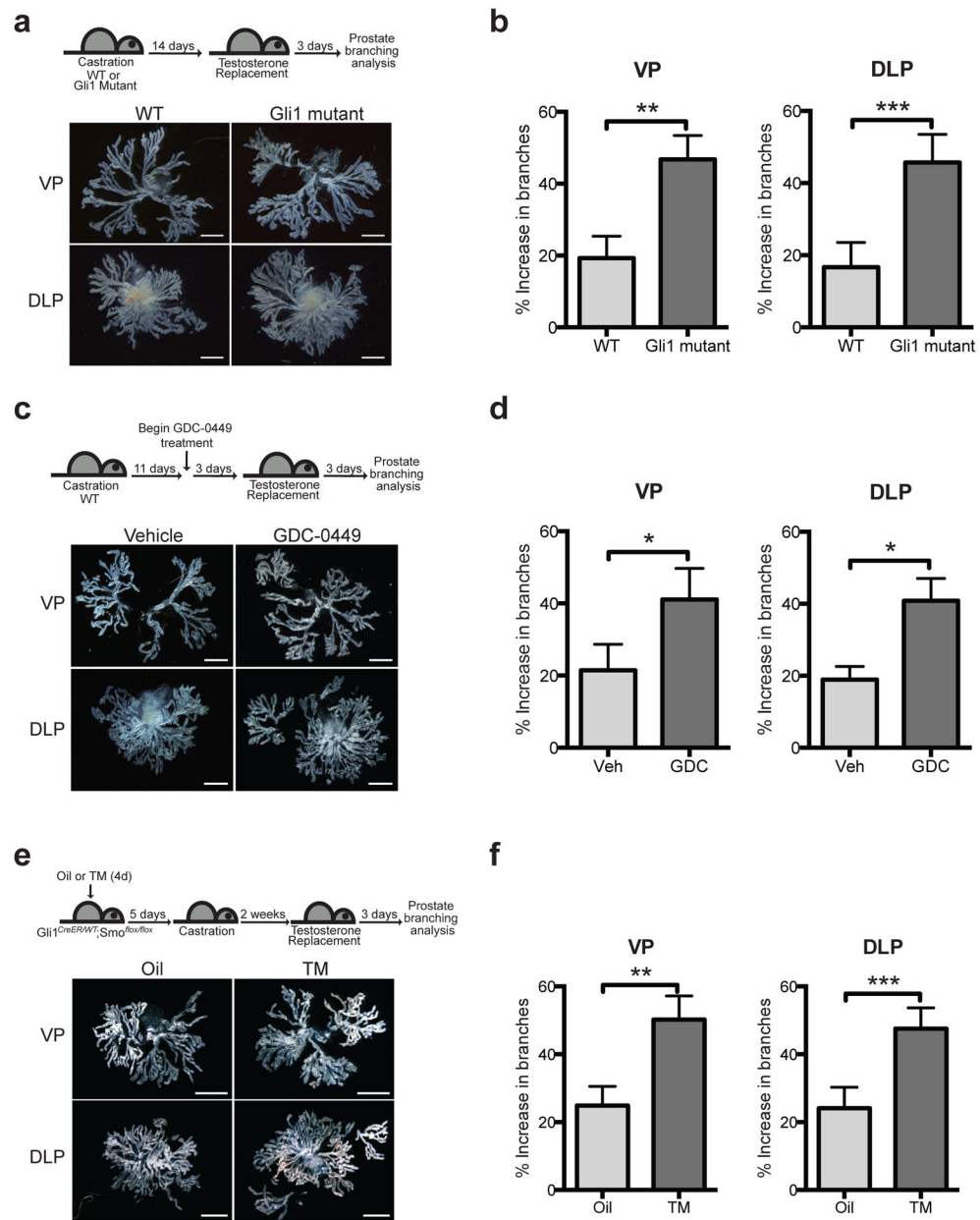
**Figure 2. Reduced Hh pathway activity increases tubulogenesis**

(a) Top: Experimental scheme describing castration and androgen replacement to compare *Gli1* mutant and wild type (WT) prostate regeneration. Bottom: Representative images from microdissections of each prostate lobe. *Gli1* mutant prostates have more branches than WT prostates. (b) *Gli1* mutant ventral prostates (VP) showed a 2.5-fold augmentation in branches relative to WT (47 vs 19 % increase in branches) after testosterone replacement. *Gli1* mutant dorsolateral prostates (DLP) showed a 2.9-fold augmentation in branching (43 vs 15 % increase in branches) after testosterone replacement. n = 6 pairs of VP or DLP. (c) Top: Experimental scheme describing the use of Hh pathway antagonist GDC-0449 (GDC) to study the effect of pathway inhibition on prostate branching in adulthood. GDC was

administered every 12 hours for 6 consecutive days. Bottom: Representative images from microdissections of each prostate lobe. GDC-treated prostates have more branches than control prostates. (d) GDC-treated VP showed a 2.0-fold augmentation of branching relative to Vehicle (Veh)-treated control (41 vs 21 % increase in branches) after testosterone replacement. GDC-treated DLP showed a 2.2-fold augmentation of branching relative to Veh-treated control (41 vs 19 % increase in branches) after testosterone replacement. n = 3 pairs of VP or DLP. (e) Top: Experimental scheme describing the administration of oil or TM to $Gli1^{CreER/WT}$; $Smo^{flox/flox}$ mice to ablate $Smo$ in the prostate stroma prior to castration and regeneration. Bottom: Representative images from microdissections of each prostate lobe. TM-treated prostates have more branches than control prostates. (f) VP from TM-treated animals showed a 2.0-fold augmentation of branching relative to Veh-treated animals (50 vs 25 % increase in branches) after testosterone replacement. DLP from TM-treated animals showed a 2.0-fold augmentation of branching relative to Veh-treated animals (48 vs 24 % increase in branches) after testosterone replacement. n = 6 pairs of VP or DLP. (b,d,f) Data are presented as mean ± s.e.m., and significance was calculated by a paired Student's t-test (*: p<0.05, **: p<0.01, ***: p<0.001). Scale bars represent 2 mm.

**Figure 3. Hh pathway activity in stromal cells leads to reduced Hgf levels**

(a) Expression of *Hgf* is 2.1-fold higher in Gli1 mutant compared to WT prostates after 3 days of testosterone replacement following castration. n=3 prostates per genotype. (b) Hgf protein levels in tissue lysates prepared from regenerating prostates, normalized to total lysate protein levels. There is a 1.2-fold increase in Hgf levels in *Gli1* mutant compared to WT VP (n=5 prostates per genotype) and a 1.9-fold increase in Hgf levels in Gli1 mutant compared to WT DLP (n=5 prostates per genotype). (c) FACS plot showing the gate drawn for sorting of basal, luminal and stromal cell populations. (d) RT-PCR analysis of RNA from each sorted fraction. *Gli1* is only expressed in the stromal cells. *Hgf* is enriched in the stromal population, and its receptor *c-Met* is enriched in the basal cell population. *CK18*, *p63* and *vimentin* are markers for the luminal, basal and stromal populations respectively. 'Total' refers to RNA extracted from dissociated unsorted adult prostate cells. (e) Immunostaining of cultured prostate stromal cells with stromal markers vimentin and smooth muscle actin (SMA). Scale bar represents 10 μm. (f) Top: Experimental scheme describing the isolation and culture of prostate stromal cells to test the effect of Hh pathway stimulation on Hgf levels *in vitro*. Bottom: Treatment of prostate stromal cells with Hh pathway agonist purmorphamine led to an increase in *Gli1* transcript levels, a 1.4-fold decrease in *Hgf* mRNA levels and a 4-fold decrease in secreted Hgf protein levels. n=4 wells per condition, one representative experiment of three is shown. (g) Top: Experimental scheme describing administration of TM to *Gli1*[CreER/WT]; *R26*[EYFP/WT] mice after testosterone replacement to label *Gli1*-positive cells during regeneration, allowing isolation of *Gli1*-positive and negative stromal cells by FACS (gated as in panel c). Bottom: RT-PCR analysis of RNA isolated from EYFP-positive and EYFP-negative stromal cells during prostate regeneration. n=3 technical replicates, one representative experiment of three is shown. (a,b,d,f,g) Data are presented as mean ± s.e.m., and significance was calculated by a unpaired Student's t-test (*: p<0.05, **: p<0.01,***: p<0.001, ****: p<0.0001).
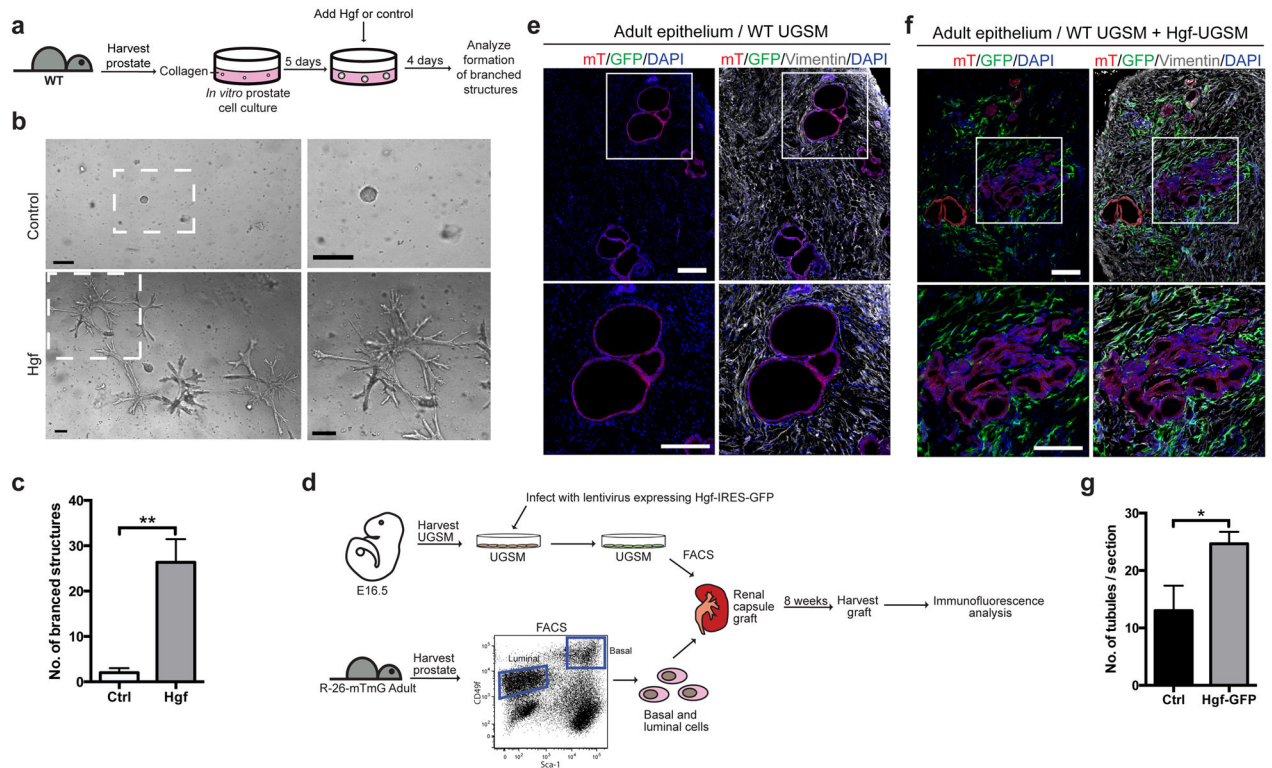
**Figure 4. Hgf induces prostate branching**

(a) Experimental scheme describing the isolation and culture of prostate cells *in vitro* until they form spheres, then treatment of the spheres with recombinant Hgf protein or a control to determine if Hgf is able to induce branching. (b) Dissociated adult prostate cells were cultured *in vitro* for 5 days, then Hgf or a vehicle control was added to the media. 4 days after addition of Hgf, branched structures were observed, but were absent in the control-treated wells. The boxed area is shown enlarged on the right. Scale bars represent 200 μm. One representative of three is shown. (c) Quantification of the total number of branched structures formed in each well. n=3 wells per condition, one representative experiment of three is shown. (d) Experimental scheme to test the ability of Hgf to induce branching in renal capsule prostate reconstitution assays. Urogenital sinus mesenchyme (USGM) was harvested from E16.5 WT embryos, infected with lentivirus expressing Hgf and GFP, GFP-positive and GFP-negative cells isolated by FACS, combined with epithelial cells from *R26*^mTmG mice, and inserted under the kidney capsule of *SCID/SCID* mice. Grafts were harvested after 8 weeks, and analyzed by immunofluorescence. (e,f) Sections through a renal capsule graft. The boxed regions are shown enlarged at the bottom. Scale bars represent 200 μm. (e) Control graft formed from adult epithelium expressing membrane-tagged tdTomato (mT) and WT uninfected urogenital sinus mesenchyme (UGSM). (f) Graft formed from adult epithelium expressing mT and equal proportions of UGSM infected with lentivirus expressing Hgf-GFP and uninfected UGSM. (g) Quantification of the number of tubules observed in each optical section through a graft. 1.9-fold more tubules were observed in grafts formed from UGSM infected with lentivirus expressing Hgf-GFP as compared to Ctrl. n=3 sections per graft. One representative experiment of two is shown. (c,g) Data are

presented as mean ± s.e.m., and significance was calculated by a unpaired Student's t-test (*: p<0.05)
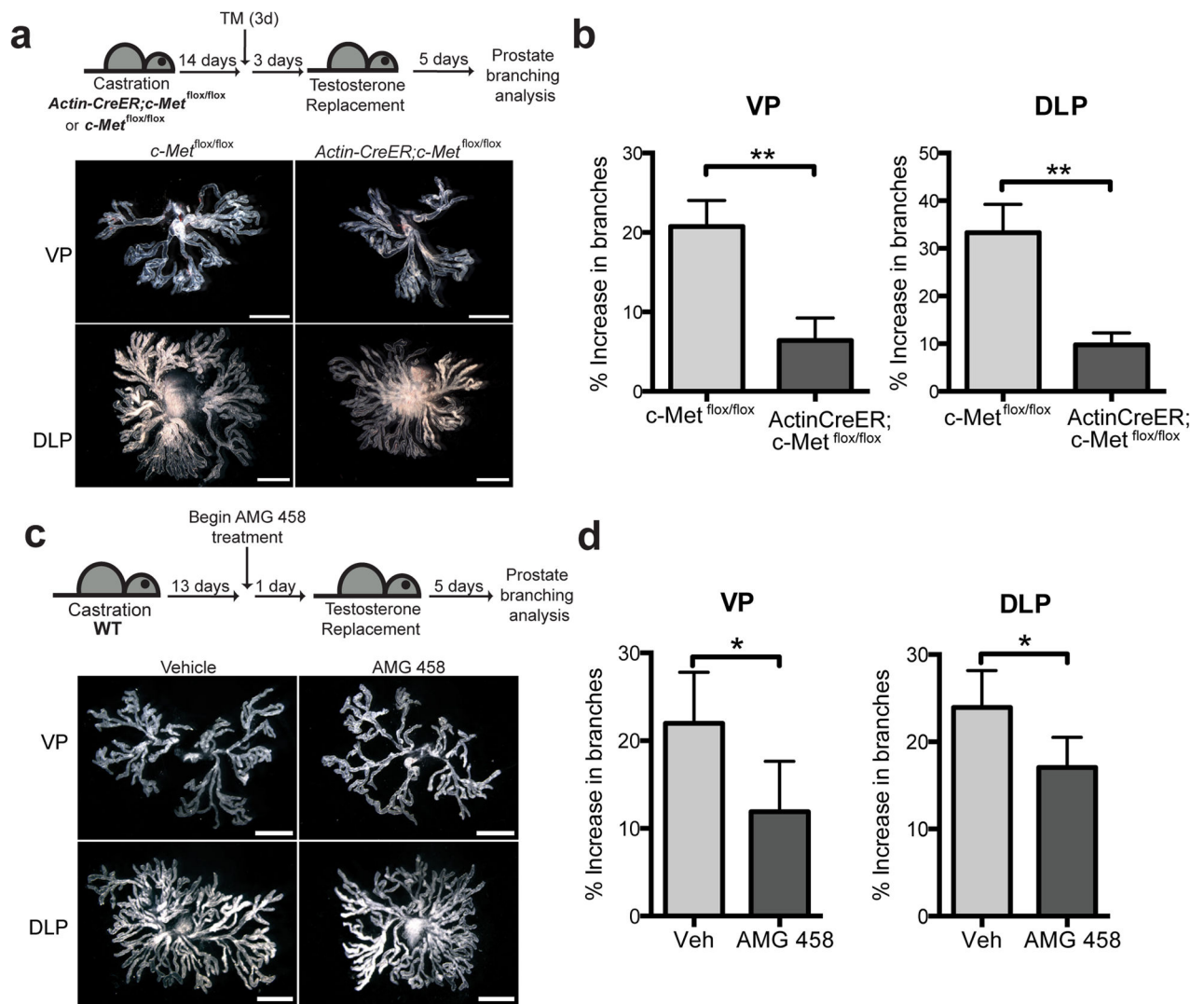
**Figure 5. Suppression of Hgf response inhibits prostate branching**

(a) Top: Schematic diagram illustrating the experimental strategy used to determine the effect of c-Met ablation on prostate regeneration. Bottom: Representative images from microdissections of each prostate lobe. *ActinCreER; c-Met*[flox/flox] prostates have fewer branches than *c-Met*[flox/flox] prostates. (b) *ActinCreER; c-Met*[flox/flox] VP showed 3.7-fold attenuation relative to *c-Met*[flox/flox] VP (6 vs 21 % increase in branches) 5 days after testosterone replacement.. *ActinCreER; c-Met*[flox/flox] DLP showed 3.3-fold attenuation relative to *c-Met*[flox/flox] DLP (10 vs 33 % increase in branches) 5 days after testosterone replacement. n=6 pairs of VP or DLP. (c) Top: Experimental scheme describing the use of c-Met inhibitor AMG 458 to study the effect of Hgf pathway inhibition on prostate branching. Starting 24 hours before testosterone replacement, AMG 458 was administered every 12 hours for 6 consecutive days. Bottom: Representative images from microdissections of each prostate lobe. AMG 458-treated prostates have more branches than vehicle-treated prostates. (d) AMG 458-treated VP showed 1.8-fold attenuation relative to vehicle (veh)-treated VP (12 vs 22 % increase in branches) 5 days after testosterone replacement. AMG 458-treated

DLP showed 1.4-fold attenuation relative to veh-treated DLP (17 vs 24 % increase in branches) 5 days after testosterone replacement. n=5 pairs of VP or DLP. (b,d) Data are presented as mean ± s.e.m., significance was calculated by a paired Student's t-test (*: $p < 0.05$, **: $p < 0.01$).
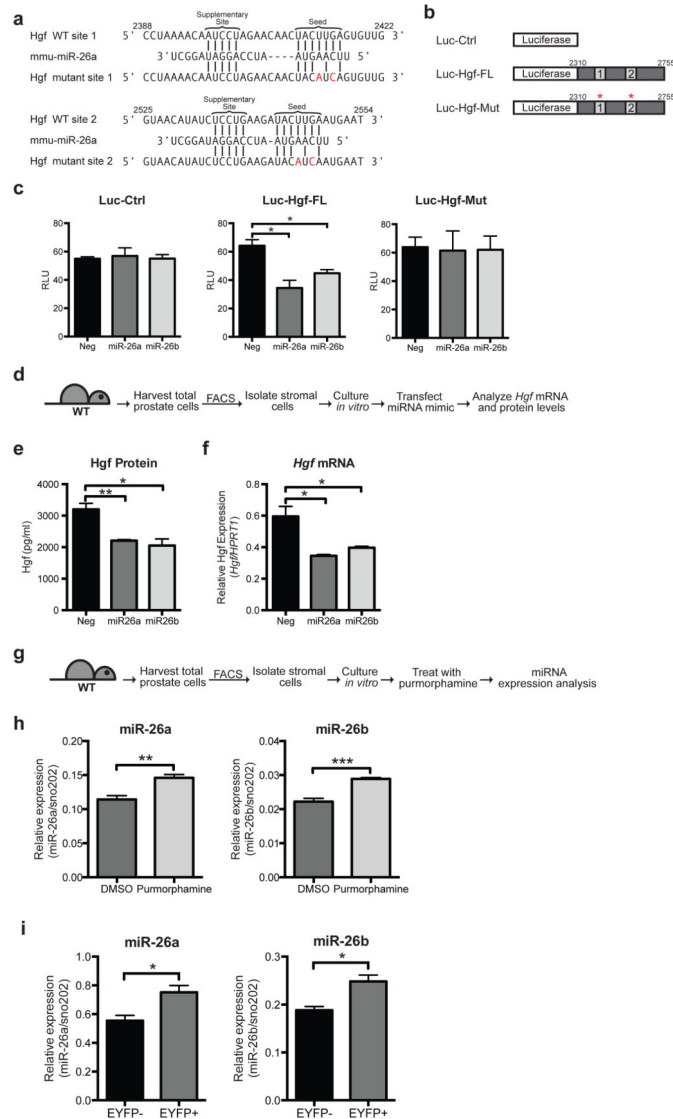
**Figure 6. Hh pathway down-regulates Hgf via miR-26a and miR-26b**

(a) Schematic representation of two predicted miR-26a target sites within the Hgf 3′UTR. Vertical lines indicate Watson-Crick pairing. Two nucleotides were mutated in each target site. Numbers indicate positions of nucleotides in the reference sequence (NM_010427). (b) pMir-Report luciferase vectors used to test if miR-26a/b target the Hgf 3′UTR. Luc-Ctrl contains the luciferase gene only. Luc-Hgf-FL contains the luciferase gene with the entire Hgf 3′UTR. Luc-Hgf-Mut contains the luciferase gene with the entire Hgf 3′UTR, with two nucleotides mutated in both sites (a). (c) Vectors in (b) were transfected into HEK293S cells with miR-26a or miR-26b mimics or a control scrambled (Neg) miRNA, and the pRL-SV40 Renilla luciferase vector. The y-axis shows luciferase normalized to renilla activity. Data are mean ± s.e.m. of separate transfections (n = 3). Transfection of miR-26a or miR-26b led to a 45% and 30% decrease in luciferase activity of Luc-Hgf-FL but not Luc-Ctrl or Luc-Hgf-Mut compared to the control. One representative experiment of three is shown. (d) Experimental scheme to test the effect of miR-26a or miR-26b on Hgf levels in primary

prostate stromal cells. (e) Transfection of miR26a or miR26b mimics led to a 30% and 31% decrease in Hgf protein secreted into the media, and a 40% and 30% decrease in Hgf transcripts respectively (f). (e,f) n=3 wells per condition, one representative experiment of three shown. (g) Experimental scheme to test the effect of purmorphamine on miR-26a and miR-26b levels in prostate stromal cells. (h) Treatment with purmorphamine led to a 1.2-fold increase in miR-26a levels and a 1.3-fold increase in miR-26b levels compared to control (DMSO). n=3 wells per condition, one representative experiment of three shown. (i) RT-PCR analysis of RNA isolated from EYFP-positive (EYFP+) and EYFP• negative (EYFP−) stromal cells from $Gli1^{CreER/WT}$; $R26^{EYFP/WT}$ prostates during regeneration (see Fig. 3g). EYFP+ cells express higher levels of miR-26a and miR-26b than EYFP− cells. n=3 technical replicates, one representative experiment of three is shown. (c,e,f,h,i) Data are presented as mean ± s.e.m., significance was calculated by a unpaired Student's t-test (*: p<0.05, **: p<0.01,***:p<0.001).
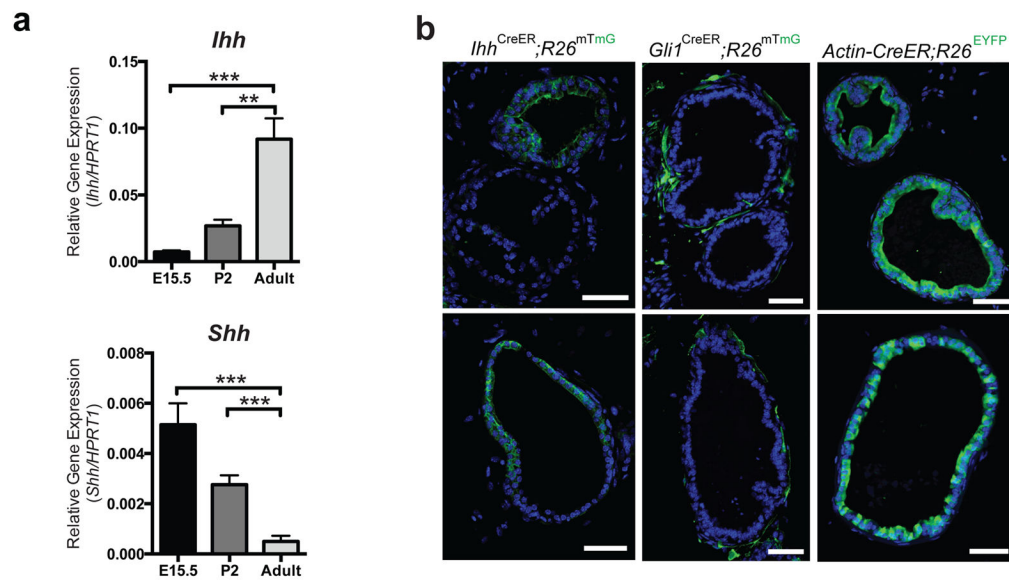
**Figure 7. *Ihh* expression patterns stromal Hh response**

(a) RT-PCR analysis of *Shh* or *Ihh* expression in the E15.5 urogenital sinus (UGS), P2 prostate and adult prostate. *Shh* is expressed 10-fold lower in adult prostate than in the UGS, and 5.5-fold lower in the adult than in the P2 prostate. *Ihh* is expressed 12-fold higher in the adult prostate than in the UGS, and 3.4-fold higher in the adult than in the P2 prostate. n=3 prostates per sample (E15.5, P2, or adult). Data are presented as mean ± s.e.m., and significance was calculated by an unpaired Student's t-test (**: $p<0.01$, ***: $p<0.001$). (b) Prostate sections from *Ihh*^CreER/WT; *R26*^mTmG/WT or *Gli1*^CreER/WT; *R26*^mTmG/WT or *Actin-CreER; R26*^EYFP/WT mice treated with TM for 4 days, and dissected 5 days later. Scale bars represent 50 μm. One representative experiment of three is shown.
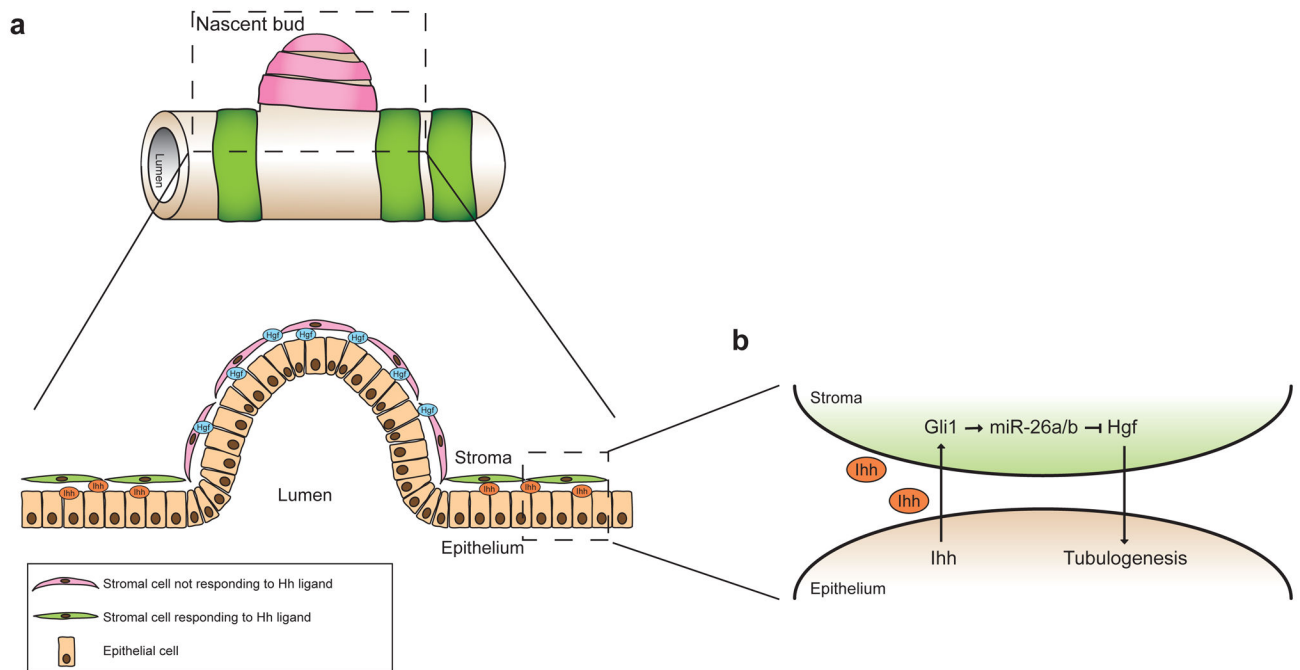
**Figure 8. Model of the spatial regulation of branching by Hh and Hgf signaling**
(a) Cartoon of a section of a prostate tubule with a nascent bud. Green bands represent Hh-responsive stromal cells and pink bands represent stromal cells that are not responding to the Hh ligand. A lateral-section through the boxed region is shown below. (b) Enlarged view of the epithelial-stromal interaction in the boxed region. In regions that are not undergoing branching, Ihh secreted by epithelial cells induces expression of *Gli1* in the adjacent stromal cells, which increases expression of miR-26a and miR-26b, which inhibit Hgf production, thereby preventing tubulogenesis. In regions lacking Ihh expression, surrounding stromal cells do not respond to the Hh ligand, hence Hgf levels are high and branching is induced.